### Title

PET/MRI of metabolic activity in osteoarthritis: A feasibility study




### Journal

Journal of Magnetic Resonance Imaging, 45(6)

### ISSN

1053-1807



### Authors

Kogan, Feliks
Fan, Audrey P
McWalter, Emily J
et al.



### Publication Date

2017-06-01

### DOI

10.1002/jmri.25529

Peer reviewed

HHS Public Access

Author manuscript

*J Magn Reson Imaging*. Author manuscript; available in PMC 2018 June 01.

Published in final edited form as:

*J Magn Reson Imaging*. 2017 June ; 45(6): 1736–1745. doi:10.1002/jmri.25529.

# PET/MR Imaging of Metabolic Activity in Osteoarthritis: A Feasibility Study

**Feliks Kogan, Ph.D.**[1], **Audrey P. Fan, Ph.D.**[1], **Emily McWalter, Ph.D.**[2], **Edwin Oei, M.D., Ph.D.**[3], **Andrew Quon, M.D.**[1], and **Garry E. Gold, M.D.**[1,4,5]

[1]Department of Radiology, Stanford University, Stanford, California, USA [2]Department of Mechanical Engineering, University of Saskatchewan, Saskatoon, Canada [3]Department of Radiology & Nuclear Medicine, Erasmus MC, University Medical Center, Rotterdam, Netherlands [4]Department of Bioengineering, Stanford University, Stanford, California, USA [5]Department of Orthopaedic Surgery, Stanford University, Stanford, California, USA

## Abstract

**Purpose—**To evaluate PET/MR knee imaging to detect and characterize osseous metabolic abnormalities and correlate PET radiotracer uptake with osseous abnormalities and cartilage degeneration observed on MRI.

**Material and Methods—**Both knees of 22 subjects with knee pain or injury were scanned at one time point, without gadolinium, on a hybrid 3.0T PET-MRI system following injection of $^{18}$F-fluorideor $^{18}$F-fluorodeoxyglucose (FDG). A musculoskeletal radiologist identified volumes of interest (VOI) around bone abnormalities on MR images and scored bone marrow lesions (BMLs) and osteophytes using a MOAKS scoring system. Cartilage appearance adjacent to bone abnormalities was grade with an MRI-modified Outerbridge classifications. On PET standardized uptake values (SUV) maps, VOIs with SUV greater than 5 times the SUV in normal appearing bone were identified as high uptake VOI ($VOI_{High}$). Differences in $^{18}$F-fluoride uptake between bone abnormalities, BML and osteophyte grades, and adjacent cartilage grades on MRI were identified using Mann-Whitney U tests.

**Results—**$SUV_{max}$ in all subchondral bone lesions (BML, Osteophytes, Sclerosis) was significantly higher than that of normal appearing bone on MRI ($p<0.001$ for all). Of the 172 high uptake regions on $^{18}$F-fluoride PET, 63 (37%) corresponded to normal-appearing subchondral bone on MRI. Furthermore, many small grade 1 osteophytes [40 of 82 (49%)], often described as the earliest signs of OA, did not show high uptake. Lastly, PET $SUV_{max}$ in subchondral bone adjacent to grade 0 cartilage was significantly lower compared to that of grade 1-2 ($p<0.05$) and grade 3-4 cartilage ($p<0.001$).

**Conclusion—**PET/MRI can simultaneously assess multiple early metabolic and morphologic markers of knee OA across multiple tissues in the joint. Our findings suggest that PET/MR may detect metabolic abnormalities in subchondral bone, which appear normal on MRI.

Corresponding Author: Feliks Kogan, PhD, Stanford University, Department of Radiology, 1201 Welch Rd, Stanford, CA 94305, fkogan@stanford.edu, 585.733.8684.

**Keywords**

Osteoarthritis; PET/MRI; Bone Remodeling

## Introduction

Osteoarthritis (OA) is a chronic, degenerative disease of the joint that affects 14 million Americans, causing joint pain, stiffness and loss of mobility (1). Despite its widespread prevalence and high societal cost, the pathogenesis of the disease remains poorly understood. Furthermore, there are no disease-modifying treatments in part because we lack the tools to effectively assess early progression.

OA is characterized by degeneration affecting all tissues in the joint, and an optimal imaging tool to study OA must be sensitive both to bone and soft tissue health. Magnetic resonance imaging (MRI) provides excellent high-resolution morphologic information of joint tissue (2), and great advances have been made to study damage to articular cartilage, meniscus and ligaments in OA. Quantitative MRI of tissue microstructure in OA, including $T_2$ or $T_{1\rho}$ relaxation times, has shown that early biochemical changes in OA can be detected before tissue loss has occurred, but has primarily focused on soft tissue (3-5). In contrast, bone metabolism cannot be directly measured using MRI.

Changes in bone metabolism are known to occur with OA, particularly in the subchondral region (6), but have received limited attention in the literature. Unlike many soft tissues in the joint, subchondral bone is a highly vascularized and metabolically active tissue that undergoes continuous remodeling (6). Bone remodeling serves to adjust bone architecture to meet changing mechanical loads on the joint, to repair micro-damage in the bone matrix, as well as to respond to trauma or bone pathology (7,8). While this subchondral bone remodeling is important to normal joint function, increased bone remodeling has been linked to the progression of OA, particularly in the early stages of the disease (6,9). Subchondral bone pathology has also been associated with cartilage loss in OA progression (10,11).

Inflammatory processes have been cited as a possible mechanism of OA tissue degeneration. In particular, bone marrow lesions (BMLs) have been strongly associated with knee pain (12), and joint space narrowing (13). However, these lesions are heterogeneous and their multifactorial etiology and pathogenesis are still poorly understood.

PET/MRI systems allow for comprehensive imaging of the whole joint, including soft tissues and bone, which is necessary to study complex disease processes in OA (14,15). This presents an opportunity to simultaneously assess the role of metabolic activity in OA with PET markers, and relate them to qualitative MRI metrics of bone pathologies in OA. Additionally, it allows for the assessment of spatial relationships between subchondral bone remodeling and cartilage health.

Several commercially available PET radiotracers are promising for studying metabolic processes in OA. $^{18}$F-fluoride is a long recognized bone-seeking agent that is able to probe bony remodeling (16-18). Additionally, fluorodeoxyglucose ($^{18}$F-FDG) PET is a widely

used marker for glucose metabolism and is sensitive to areas of acute phase cellular response (neutrophils or PMNs), such as inflammation (19).

The purpose of our study was to investigate the potential of PET/MR knee imaging to detect and characterize osseous metabolic abnormalities in patients with knee pain or prior injury and correlate degenerative bone and cartilage findings on MRI with subchondral $^{18}$F-fluoride uptake on PET.

## Materials and Methods

### Study population

From September 2014 to July 2016, 22 patients with a prior history of knee injury or pain were recruited for the study. Subjects with known high grade OA, pregnant women and children were excluded from participating. Prior to participating in the study, all subjects were informed about the nature of the study and provided consent according to the University Institutional Review Board. The study was Health Insurance Portability and Accountability Act (HIPAA) – compliant.

### PET-MRI Scanning

Both knees of each subject were scanned on a 3T whole-body time-of-flight PET-MR hybrid system (GE Healthcare, Milwaukee, WI) following injection of 2-5 mCi of $^{18}$F-fluoride and a 45-minute delay to allow for tracer uptake. In addition, 3 subjects received a second PET/MRI scan on a separate day using injection of 5 mCi of $^{18}$F-FDG and a 60-minute uptake delay.

PET data acquisition of the knee was performed in one PET bed (FOV = 26 cm). MRI data was simultaneously acquired on each knee with a 16-channel flexible phased-array wrap coil (NeoCoil, Pewaukee, WI). Scans sensitive to bone marrow lesions were acquired using fat-suppressed, fast spin-echo (FSE) sequences: TR: 2500 ms, FOV: 16×16 cm, matrix size: 320 × 224, slice thickness: 3 mm, echo train length: 12, TE: 30 ms (Proton Density-weighted), 54 ms (T2-weighted). A zero echo time (zTE) (20) sequence was used to identify osteophytes: TR: 2500 ms, TE: 12 μs, FOV: 18×18 cm, flip angle: 3°, resolution: 0.8 mm isotropic. To assess subchondral sclerosis, fat-water separated images were acquired using an IDEAL FSE sequence (21): TR: 3000 ms, TE: 30 ms, FOV: 16×16 cm, matrix size: 320 × 256, slice thickness: 3 mm, echo train length: 8, phase acceleration: 2. Finally, a Dixon fat-water sequence was run for MR-based attenuation correction (MRAC) of PET photons (22). MRAC uses an automated anatomic segmentation and assigns tissue-specific linear attenuation coefficients to each segmented tissue. PET data was acquired simultaneously for the entire duration of the MRI scan. The scan time for each knee was 30 minutes for a total scan time of roughly one hour.

### Image Analysis

A musculoskeletal radiologist with 22 years of experience (G.G.) identified volumes of interest (VOI) around bone abnormalities on MR images. This included “bone marrow lesions” (BMLs) identified as areas of high $T_2$ signal in subchondral bone (23), osteophytes

identified as bony protrusions on zTE MR images, and subchondral sclerosis, identified as subchondral bone with low signal intensity on both fat-saturated $T_2$-weighted FSE images and Dixon fat images (23). Additionally, BMLs and osteophytes were scored according to MRI Osteoarthritis Knee Score (MOAKS) (24). For both $^{18}$F-fluoride and $^{18}$F-FDG PET acquisitions, Standardized Uptake Values (SUV) images were reconstructed from list-mode data onto a 192 × 192 matrix using time-of-flight PET reconstruction. VOIs with SUV greater than 5 times the reference SUV in normal bone (i.e., the mean SUV from a region of normal-appearing trabecular bone in the medial femoral condyle) were identified as high uptake VOI ($VOI_{High}$) on PET SUV maps. Furthermore, $SUV_{max}$ from $VOI_{High}$ that did not correspond to any MRI findings were identified. Lastly, cartilage adjacent to identified areas of bone abnormalities and $VOI_{High}$ was graded by a radiologist (G.G.) according to an MRI-modified Outerbridge classification [*Grade 0* – Normal appearing cartilage; *Grade 1* - Signal intensity alterations with no loss of cartilage thickness; *Grade 2* - Shallow superficial ulceration, fibrillation, or fissuring involving less than 50% of the depth of the articular surface; *Grade 3* - Deep ulceration, fibrillation, fissuring or a chondral flap involving 50% depth or more of the articular cartilage without exposure of subchondral bone; *Grade 4* - Full-thickness chondral wear with exposure of subchondral bone] (25,26).

We tested the hypothesis that maximum SUV ($SUV_{max}$) on PET images differed between different bone pathologies (identified on MRI) as well as from normal-appearing bone using the Mann-Whitney U test. Similarly, differences in $^{18}$F-fluoride PET uptake related to BML and osteophyte grades identified on MRI using a Mann-Whitney U test with Bonferroni correction. Lastly, differences in $^{18}$F-fluoride PET uptake for different adjacent cartilage grades determined from MR images using a Mann-Whitney U test with Bonferroni Correction. All statistical analyses were performed using the statistical toolbox for Matlab (Mathworks, Natick, MA) and *p*-values less than 0.05 were considered statistically significant.

## Results

All subjects had subchondral bone and cartilage features of OA as identified on MRI. 22 subjects (mean age 36.8 ± 14.8 years, 16 male, 6 female) were included in the study with a mean BMI of 26.1 ± 4.1 kg/m$^2$. In the 44 knee joints analyzed in our study, 34 BMLs [14-Grade 1 (41%); 16-Grade 2 (47%); 4-Grade 3 (12%)], 103 osteophytes [82-Grade 1 (80%); 15-Grade 2 (15 %), 6-Grade 3 (6%)], and 13 areas of subchondral sclerosis were identified on MRI and graded using a MOAKS classification. Additionally, 172 PET positive regions of $VOI_{High}$ were identified on $^{18}$F-fluoride PET. In the regions adjacent to MRI abnormalities or $VOI_{high}$ PET findings, MRI grading of cartilage lesions revealed 56 areas of normal appearing cartilage (grade 0), 124 areas of mild degeneration (grades 1-2) and 41 areas of severe degeneration (grade 3-4). In the three patients (ages 52, 36, 23; corresponding BMI 31.3, 26, 24.4; all male) who were scanned with both tracers, 10 BMLs were identified on MRI. Additionally, in one of these patients (age 23, BMI 24.4), who had undergone anterior cruciate ligament (ACL) reconstruction, two regions of increased $^{18}$F-FDG uptake ($VOI_{High}$) were observed around their ACL graft and meniscus, respectively.

Figure 1 displays are presentative PET and MRI image of a BML (blue arrowhead), osteophytes (red diamond arrows), on MRI co-localized with high uptake on $^{18}$F-fluoride PET. Similarly, an example of subchondral sclerosis (gray solid arrows) and an osteophyte (red diamond arrow) on MRI corresponding to high uptake on $^{18}$F-fluoride PET is seen in Figure 2. The mean $SUV_{max}$ on PET in lesion VOIs identified on MRI was 12.4±6.7 for BMLs, 5.7±3.3 for osteophytes, 6.5±3.2 for sclerosis. In comparison, the mean $SUV_{max}$ from regions of normal-appearing bone from the medial femoral condyle was 1.1 ± 0.3. BMLs observed on $T_2$-weighted FSE images consistently correlated with high $^{18}$F-fluoride PET uptake identified as $VOI_{High}$ [33 of 34 (97%)] (Table 1). Furthermore, $SUV_{max}$ in BMLs was significantly higher than that of osteophytes and subchondral sclerosis ($p<0.001$ for both) (Figure 3). $SUV_{max}$ in all subchondral bone lesions (BML, Osteophytes, Sclerosis) was significantly higher than that of normal appearing bone on MRI ($p<0.001$ for all).

BMLs with higher MOAKS score on MRI showed higher $^{18}$F-fluoride uptake on PET (Figure 4a). Mean $SUV_{max}$ of 7.7±1.6, 13.2±3.5, 25.4±8.9 were observed in grade 1, grade 2 and grade 3 BMLs, respectively (Figure 4a). Grade 2 and grade 3 BMLs both showed significantly higher $SUV_{max}$ than grade 1 BMLs ($p<0.001$ for both). All grade 2 [16 of 16 (100%)] and grade 3 [4 of 4 (100%)] BMLs identified on MRI corresponded to $VOI_{High}$ identified on $^{18}$F-fluoride PET, and the concordance in grade 1 BMLs was also high [13 of 14 (93%)].

Associations between $^{18}$F-fluoride $VOI_{High}$ and MRI findings of osteophytes [60 of 103 (58%)] and subchondral sclerosis [8 of 13 (62%)] were less consistent. However, similar to BMLs, osteophytes with higher grades as determined by MOAKS score on MRI had a higher mean $SUV_{max}$ on PET scans (Figure 4b). Mean $SUV_{max}$ values of 4.6±2.3, 9.4±3.2, 10.8±3.3 were observed in grade 1, grade 2 and grade 3 osteophytes, respectively. Grade 2 and grade 3 osteophytes also showed significantly higher $SUV_{max}$ than grade 1 osteophytes ($p<0.001$ for both). Additionally, many small grade 1 osteophytes did not show high uptake on $^{18}$F-fluoride PET (Figure 5). While concordance with high uptake on $^{18}$F-fluoride PET was observed between most grade 2 [14 of 15 (93%)] and all grade 3 [6 of 6 (100%)] osteophytes identified on MRI, fewer than half [40 of 82 (49%)] of the grade 1 osteophytes identified on MRI corresponded to high uptake on $^{18}$F-fluoride PET.

High $^{18}$F-fluoride uptake in subchondral bone did not always correspond to structural abnormalities detected on MRI (Figure 1 & Figure 6 - purple arrows). Of the 172 regions of $VOI_{High}$ identified on $^{18}$F-fluoride PET, 109 (63%) corresponded to MRI findings while 63 $VOI_{High}$ (37%) corresponded to normal-appearing subchondral bone on MRI.

Differences were also observed between $SUV_{max}$ and adjacent cartilage grade. Mean $SUV_{max}$ increased with cartilage grade from 5.9±3.3 in normal-appearing (grade 0) cartilage; to 7.6±4.3 in mildly degenerated (grade 1-2) cartilage; to 9.5±5.3 in severely degenerated (grade 3-4) cartilage (Figure 7). Significant differences were observed between PET $SUV_{max}$ in subchondral bone adjacent to grade 0 cartilage compared to grade 1-2 ($p<0.05$) and grade 3-4 cartilage ($p<0.001$) as well as between grade 1-2 and grade 3-4 cartilage ($p<0.05$). Additionally, differences were observed between the mean cartilage

grade adjacent to BMLs (2.3±1.0), osteophytes (1.5±1.1), and regions of high uptake with no associated subchondral bone MRI findings (1.1±1.1).

Uptake of $^{18}$F-FDG in subchondral BMLs was substantially lower than that of $^{18}$F-fluoride. In the 10 BMLs evaluated with both radiotracers, none corresponded to $VOI_{High}$ on $^{18}$F-FDG PET while all 10 BMLs corresponded to $VOI_{High}$ on $^{18}$F-fluoride PET. All nine BMLs identified on MRI as grade 1 or grade 2 had FDG $SUV_{max}$ comparable to that of normal-appearing bone (0.6-0.7) while the solo grade 3 lesion had a slightly elevated FDG $SUV_{max}$ (1.4). Figure 8 shows a large osteophyte that has minimal $^{18}$F-FDG uptake but substantial $^{18}$F-fluoride accumulation on PET scans obtained in separate sessions. While $^{18}$F-FDG uptake did not appear elevated in areas of subchondral bone abnormalities identified on MRI, in the two regions where high $^{18}$F-FDG uptake was observed in soft tissue (ligament and meniscus), high $^{18}$F-fluoride uptake ($VOI_{High}$) was observed in adjacent subchondral bone (Figure 9).

## Discussion

Hybrid PET-MR systems allow for simultaneous, sensitive and quantitative assessment of bone, articular cartilage and other soft tissues and may be an optimal method to study OA. MRI has become the standard for evaluation of soft tissue in joints. This work shows the addition of PET provides an opportunity to concurrently measure changes in the bone metabolic activity. This combination may not only help understand bone pathology in OA but may also provide crucial information linking changes in soft tissue with bone remodeling and inflammation.

PET imaging allows for quantitative assessment of functional changes that occur in OA at the molecular level. While bony pathology has long been thought to play an important role in the development of OA, its etiology, activity, and progression is still poorly understood. This study demonstrated the sensitivity of $^{18}$F-fluoride PET to osteoblastic processes and its potential to quantitatively evaluate subchondral bone remodeling and other metabolic abnormalities in bony pathology in OA.

Findings of abnormalities that only appeared on MRI or as areas of high $^{18}$F-fluoride uptake on PET are of particular interest. Of all $VOI_{High}$ identified on $^{18}$F-fluoride PET, 37 percent corresponded to normal-appearing subchondral bone marrow on MRI. As molecular changes often precede changes at the tissue level, $^{18}$F-fluoride may serve as a marker of early bone remodeling changes that occurs before structural MRI damage is seen in the joint. This is further supported by the association of $^{18}$F-fluoride PET regions of $VOI_{High}$ with adjacent mild (grade 1-2) cartilage degeneration that was often observed on MRI. Biomarkers that effectively assess early progression of OA are crucial for the development and evaluation of disease modifying treatments, and the osteoblast activity detected on $^{18}$F-fluoride is a promising candidate.

Of equal importance, a lack of metabolic activity may indicate that certain lesions play a limited role in OA pathogenesis. While there was frequent co-localization between grade 2 (93%) and grade 3 (100%) osteophytes and MRI abnormalities, more than half of grade 1

osteophytes identified on MRI did not correlate with increased $^{18}$F-fluoride uptake. These small osteophytes are thought to be earliest signs of radiographic OA and PET data suggests their metabolic activity is not elevated. $^{18}$F-fluoride PET provides a quantitative measure to characterize these lesions and study their effect on the progression of OA.

Our $^{18}$F-fluoride results suggest that BMLs are significantly more metabolically active than osteophytes and sclerosis. Furthermore, higher $^{18}$F-fluoride PET uptake was seen in osteophytes and BMLs of higher grade identified with MRI. However, there were large standard deviations observed within each type of bone abnormalities and within lesion grade. The sensitivity of $^{18}$F-fluoride PET to bone remodeling may help us to better understand and characterize individual lesions in subchondral bone.

BMLs have been a topic of increasing interest in OA because they are considered significant sources of pain (12) and are linked to the radiographic severity of OA (27) and increased rate of OA progression (13). Despite a putative link between BMLs and symptoms of OA, current identification of BMLs as areas of high signal in bone on fat suppressed T2w images is not quantitative and often a late finding. As such, the importance of individual lesions as identified on MRI on the progression of OA is poorly understood. $^{18}$F-fluoride PET offers the ability to quantify bone remodeling and osteoblast metabolic activity in BMLs. Our $^{18}$F-fluoride findings suggest that BMLs identified on MRI are significantly more metabolically active for bone remodeling than other bone pathology (e.g. osteophytes and sclerosis) as well as normal-appearing areas on MRI. BMLs were also associated with more severe degeneration of the adjacent cartilage compared with other bone pathologies. An association between BMLs and cartilage damage is in agreement with prior literature that showed BMLs are linked with loss and degeneration of the overlying cartilage (10,28).

Another important point of discussion is the role of inflammation on BMLs in OA. In addition to degenerative arthropathies, BMLs are also associated with rheumatoid arthritis, bone trauma, as well as ischemic and neoplastic disorders (29). While previous work has demonstrated that BMLs in OA has less of an inflammatory component than in rheumatoid arthritis (30), there are varying theories about the involvement of inflammation in OA. Our early results show considerable $^{18}$F-fluoride and minimal $^{18}$F-FDG uptake in BMLs relative to normal-appearing bone, suggesting that bone remodeling processes play a larger role in these lesions compared with inflammatory processes. However, a larger study is necessary to determine uptake of $^{18}$F-FDG in these lesions. This finding agrees with prior work which showed that BMLs may not respond to anti-inflammatory treatments in knee OA (31).

One of the biggest benefits of hybrid PET-MR imaging of OA is the ability to simultaneously evaluate molecular and morphologic spatial relationships across multiple tissues. In this study, we evaluated the relationship between metabolic bony activity in subchondral bone pathology and cartilage morphology. A trend was seen between increased $^{18}$F-fluoride PET uptake and increasing structural degeneration in the adjacent cartilage as semi-quantitatively assessed using a modified Outerbridge scoring system. This finding suggests that degenerative changes and processes in bone and cartilage are linked. $^{18}$F-fluoride PET, in combination with early MRI metrics of cartilage biochemistry (32), may provide an optimal method to study relationships between adjacent tissue

degeneration in early OA. Other PET tracers, such as $^{18}$F-FDG, may provide complementary information about soft tissue inflammation, and could be utilized in combination to study OA degeneration in the entire joint.

While $^{18}$F-fluoride has been extensively used to image bone metastases, it has only more recently been applied to degenerative joint disease (33-35). Kobayashi et al. showed that increasing severity of hip pain correlated with increasing $SUV_{max}$. In addition, they showed that $SUV_{max}$ was significantly higher in hip joints with an abnormal finding in bone on MRI (33). A separate study showed subjects with patellofemoral pain exhibited elevated $^{18}$F-fluoride uptake indicative of increased bone metabolic activity at the patellofemoral joint, but did not always correspond to structural damage in the bone or cartilage on MRI (34). However, these studies performed $^{18}$F-fluoride PET and MR in separate scan sessions and did not evaluate individual bone abnormalities. Additionally, spatial relationships between subchondral bone metabolism and cartilage changes were not assessed.

Simultaneous acquisition of PET and MRI data allows for considerable reduction in scan time while obtaining registered images. Furthermore, since PET data is acquired for the duration of the MRI protocol, this permits a reduction in the dose of radiotracer needed as compared to PET-CT. In this study, because PET data was acquired for the duration of the 30-minute MRI protocol, the injected dose of $^{18}$F-Fluoride was decreased from a standard clinical dose of 5.0 mCi to 2.0 mCi while maintaining high signal-to-noise ratio in PET SUV maps. For an adult, this is an estimated effective dose of 1.4 mSv. As MRI is non-ionizing, this protocol allows for simultaneous acquisition of functional and high-resolution anatomical data with a minimal effective dose to the subject.

It is also important to point out several limitations to this study. This study used a cross-sectional analysis of subjects with knee pain and injuries. BMLs are heterogeneous with a diverse etiology and their size and features are known to change over time. We believe the BMLs in these subjects are the result of degenerative osteoarthropathy, but serial tracking of these lesions is needed to better understand the role of bone remodeling and inflammation in these pathologies. Additionally, while an association between $^{18}$F-fluoride uptake in subchondral bone and cartilage damage on MRI was observed, longitudinal studies are needed to determine the chronological order of these changes.

For imaging techniques, it should also be noted that radiographs are the standard imaging method used to detect osteophytes and subchondral sclerosis, as bone is ordinarily invisible on conventional MRI due to the extremely short life-time (T2) of its protons. However, zTE MRI allows for visualization of short T2 species such as bone, and our radiologist has over 20 years of experience identifying these lesions on MRI. Lastly, PET photon attenuation due to the flexible coil array used for MR imaging was not accounted for in calculation of PET SUV maps. This likely led to an underestimation of calculated SUV values, although we expect the tracer distributions to be preserved with and without this coil (36).

No histopathology was acquired in this study; thus, we could not confirm that high PET uptake correlated to bone pathology. Instead, we have described these as abnormalities in bone metabolism. Additionally, an asymptomatic control population with no history of knee

problems has not yet been studied. While a lack of abnormal PET or MRI findings was observed in the contralateral knee of several subjects with unilateral knee injury, more studies are needed to determine the range of PET radiotracer uptake in normal controls. Furthermore, the patient population used in this study was small and heterogeneous including a range of ages, pain, and included post-surgical patients. As a feasibility study, we felt it appropriate to study a broad range of subjects. As such, the findings of this study are observations, which highlight the potential of PET/MRI to simultaneously study multiple functional and morphologic factors in the knee. More targeted studies in homogeneous patient cohorts are needed to make conclusions about the use of $^{18}$F-fluoride or $^{18}$F-FDG as markers of OA pathogenesis.

This work presents a novel technique to simultaneously assess early metabolic and structural markers of knee OA across multiple tissues in the joint. $^{18}$F-fluoride PET/MR may detect knee abnormalities unseen on MRI alone and is a promising tool for detection of early metabolic changes in OA. Further, higher $^{18}$F-fluoride uptake corresponds to worse degeneration in the adjacent cartilage, suggesting a spatial relationship between bone remodeling and cartilage health. Use of additional tracers such as $^{18}$F-FDG PET can provide complementary information about inflammatory processes occurring in soft tissues. PET/MR thus can simultaneously assess multiple early metabolic and biochemical markers of knee OA progression across all tissues in the joint. This information may provide new insights into OA pathogenesis and lead to new treatment targets to arrest the onset and progression of OA.

## Acknowledgments

We gratefully acknowledge Dr. Mehdi Khalighi and Jorge Guzman for their help with development of techniques for hybrid PET/MR Imaging. We would also like to thank Dawn Holley and Harsh Gandhi for their help running PET/MRI Scans. Finally, we would like to recognize Dr. Jarrett Rosenberg for all his with the statistical analysis.

**Grant Support:** GE Healthcare, R01EB002524, K24AR062068

## Literature Cited

1. Deshpande BR, Katz JN, Solomon DH, Yelin EH, Hunter DJ, Messier SP, Suter LG, Losina E. The number of persons with symptomatic knee osteoarthritis in the United States: Impact of race/ethnicity, age, sex, and obesity. Arthritis care & research. 2016
2. Hayashi D, Guermazi A, Kwoh CK. Clinical and translational potential of MRI evaluation in knee osteoarthritis. Current rheumatology reports. 2014; 16(1):391. [PubMed: 24318386]
3. Williams A, Qian Y, Bear D, Chu CR. Assessing degeneration of human articular cartilage with ultra-short echo time (UTE) T2* mapping. Osteoarthritis Cartilage. 2010; 18(4):539–546. [PubMed: 20170769]
4. Matzat SJ, Kogan F, Fong GW, Gold GE. Imaging strategies for assessing cartilage composition in osteoarthritis. Current rheumatology reports. 2014; 16(11):462. [PubMed: 25218737]
5. Guermazi A, Alizai H, Crema MD, Trattnig S, Regatte RR, Roemer FW. Compositional MRI techniques for evaluation of cartilage degeneration in osteoarthritis. Osteoarthritis Cartilage. 2015; 23(10):1639–1653. [PubMed: 26050864]
6. Burr DB, Gallant MA. Bone remodelling in osteoarthritis. Nature reviews Rheumatology. 2012; 8(11):665–673. [PubMed: 22868925]
7. Robling AG, Castillo AB, Turner CH. Biomechanical and molecular regulation of bone remodeling. Annu Rev Biomed Eng. 2006; 8:455–498. [PubMed: 16834564]

8. Rucci N. Molecular biology of bone remodelling. Clin Cases Miner Bone Metab. 2008; 5(1):49–56. [PubMed: 22460846]
9. Hayami T, Pickarski M, Wesolowski GA, McLane J, Bone A, Destefano J, Rodan GA, Duong LT. The role of subchondral bone remodeling in osteoarthritis: reduction of cartilage degeneration and prevention of osteophyte formation by alendronate in the rat anterior cruciate ligament transection model. Arthritis Rheum. 2004; 50(4):1193–1206. [PubMed: 15077302]
10. Roemer FW, Guermazi A, Javaid MK, Lynch JA, Niu J, Zhang Y, Felson DT, Lewis CE, Torner J, Nevitt MC. investigators MS. Change in MRI-detected subchondral bone marrow lesions is associated with cartilage loss: the MOST Study. A longitudinal multicentre study of knee osteoarthritis. Ann Rheum Dis. 2009; 68(9):1461–1465. [PubMed: 18829615]
11. Hunter DJ, Zhang Y, Niu J, Goggins J, Amin S, LaValley MP, Guermazi A, Genant H, Gale D, Felson DT. Increase in bone marrow lesions associated with cartilage loss: a longitudinal magnetic resonance imaging study of knee osteoarthritis. Arthritis Rheum. 2006; 54(5):1529–1535. [PubMed: 16646037]
12. Felson DT, Chaisson CE, Hill CL, Totterman SM, Gale ME, Skinner KM, Kazis L, Gale DR. The association of bone marrow lesions with pain in knee osteoarthritis. Ann Intern Med. 2001; 134(7): 541–549. [PubMed: 11281736]
13. Felson DT, McLaughlin S, Goggins J, LaValley MP, Gale ME, Totterman S, Li W, Hill C, Gale D. Bone marrow edema and its relation to progression of knee osteoarthritis. Ann Intern Med. 2003; 139(5 Pt 1):330–336. [PubMed: 12965941]
14. Torigian DA, Zaidi H, Kwee TC, Saboury B, Udupa JK, Cho ZH, Alavi A. PET/MR imaging: technical aspects and potential clinical applications. Radiology. 2013; 267(1):26–44. [PubMed: 23525716]
15. Lee IS, Jin YH, Hong SH, Yang SO. Musculoskeletal applications of PET/MR. Semin Musculoskelet Radiol. 2014; 18(2):203–216. [PubMed: 24715451]
16. Blau M, Nagler W, Bender MA. Fluorine-18: a new isotope for bone scanning. Journal of nuclear medicine : official publication, Society of Nuclear Medicine. 1962; 3:332–334.
17. Jadvar H, Desai B, Conti PS. Sodium 18F-fluoride PET/CT of bone, joint, and other disorders. Semin Nucl Med. 2015; 45(1):58–65. [PubMed: 25475379]
18. Ohnona J, Michaud L, Balogova S, Paycha F, Nataf V, Chauchat P, Talbot JN, Kerrou K. Can we achieve a radionuclide radiation dose equal to or less than that of 99mTc-hydroxymethane diphosphonate bone scintigraphy with a low-dose 18F-sodium fluoride time-of-flight PET of diagnostic quality? Nucl Med Commun. 2013; 34(5):417–425. [PubMed: 23470463]
19. Hong YH, Kong EJ. (18F)Fluoro-deoxy-D-glucose uptake of knee joints in the aspect of age-related osteoarthritis: a case-control study. BMC musculoskeletal disorders. 2013; 14:141. [PubMed: 23607872]
20. Gurney PT, Hargreaves BA, Nishimura DG. Design and analysis of a practical 3D cones trajectory. Magn Reson Med. 2006; 55(3):575–582. [PubMed: 16450366]
21. Reeder SB, McKenzie CA, Pineda AR, Yu H, Shimakawa A, Brau AC, Hargreaves BA, Gold GE, Brittain JH. Water-fat separation with IDEAL gradient-echo imaging. J Magn Reson Imaging. 2007; 25(3):644–652. [PubMed: 17326087]
22. Wagenknecht G, Kaiser HJ, Mottaghy FM, Herzog H. MRI for attenuation correction in PET: methods and challenges. Magma. 2013; 26(1):99–113. [PubMed: 23179594]
23. Roemer FW, Frobell R, Hunter DJ, Crema MD, Fischer W, Bohndorf K, Guermazi A. MRI-detected subchondral bone marrow signal alterations of the knee joint: terminology, imaging appearance, relevance and radiological differential diagnosis. Osteoarthritis Cartilage. 2009; 17(9): 1115–1131. [PubMed: 19358902]
24. Hunter D, Guermazi A, Lo G, Grainger A, Conaghan P, Boudreau R, Roemer F. Evolution of semi-quantitative whole joint assessment of knee OA: MOAKS (MRI Osteoarthritis Knee Score). Osteoarthritis and Cartilage. 2011; 19(8):990–1002. [PubMed: 21645627]
25. Outerbridge RE. The etiology of chondromalacia patellae. J Bone Joint Surg Br. 1961; 43-B:752–757. [PubMed: 14038135]

26. Potter HG, Linklater JM, Allen AA, Hannafin JA, Haas SB. Magnetic resonance imaging of articular cartilage in the knee. An evaluation with use of fast-spin-echo imaging. The Journal of bone and joint surgery American volume. 1998; 80(9):1276–1284. [PubMed: 9759811]
27. Link TM, Steinbach LS, Ghosh S, Ries M, Lu Y, Lane N, Majumdar S. Osteoarthritis: MR imaging findings in different stages of disease and correlation with clinical findings. Radiology. 2003; 226(2):373–381. [PubMed: 12563128]
28. Muratovic D, Cicuttini F, Wluka A, Findlay D, Wang Y, Otto S, Taylor D, Humphries J, Lee Y, Labrinidis A, Williams R, Kuliwaba J. Bone marrow lesions detected by specific combination of MRI sequences are associated with severity of osteochondral degeneration. Arthritis research & therapy. 2015; 18:54.
29. Starr AM, Wessely MA, Albastaki U, Pierre-Jerome C, Kettner NW. Bone marrow edema: pathophysiology, differential diagnosis, and imaging. Acta Radiol. 2008; 49(7):771–786. [PubMed: 18608031]
30. Elzinga EH, van der Laken CJ, Comans EF, Lammertsma AA, Dijkmans BA, Voskuyl AE. 2-Deoxy-2-[F-18]fluoro-D-glucose joint uptake on positron emission tomography images: rheumatoid arthritis versus osteoarthritis. Molecular imaging and biology : MIB : the official publication of the Academy of Molecular Imaging. 2007; 9(6):357–360. [PubMed: 17902022]
31. O'Neill TW, Parkes MJ, Maricar N, Gait AD, Cootes TF, Marjanovic EJ, Bailey D, Hutchinson CE, Felson DT. Bone marrow lesions may not respond to anti-inflammatory treatments in knee osteoarthritis(OA). Osteoarthritis and Cartilage. 2014; 22:S475.
32. Oei EH, van Tiel J, Robinson WH, Gold GE. Quantitative radiological imaging techniques for articular cartilage composition: Towards early diagnosis and development of disease-modifying therapeutics for osteoarthritis. Arthritis care & research. 2014
33. Kobayashi N, Inaba Y, Tateishi U, Ike H, Kubota S, Inoue T, Saito T. Comparison of 18F-fluoride positron emission tomography and magnetic resonance imaging in evaluating early-stage osteoarthritis of the hip. Nucl Med Commun. 2015; 36(1):84–89. [PubMed: 25230054]
34. Draper CE, Quon A, Fredericson M, Besier TF, Delp SL, Beaupre GS, Gold GE. Comparison of MRI and (1)(8)F-NaF PET/CT in patients with patellofemoral pain. J Magn Reson Imaging. 2012; 36(4):928–932. [PubMed: 22549985]
35. Lee JW, Lee SM, Kim SJ, Choi JW, Baek KW. Clinical utility of fluoride-18 positron emission tomography/CT in temporomandibular disorder with osteoarthritis: comparisons with 99mTc-MDP bone scan. Dento maxillo facial radiology. 2013; 42(2):29292350. [PubMed: 23393302]
36. Kogan, F., Rosenberg, J., Brazina, S., Fan, A., Holley, D., Gold, G. Effect of 16-Channel Flex Array Coil on PET Standardized Uptake Values for PET/MR Imaging of the knee. Toronto, Canada: 2015.

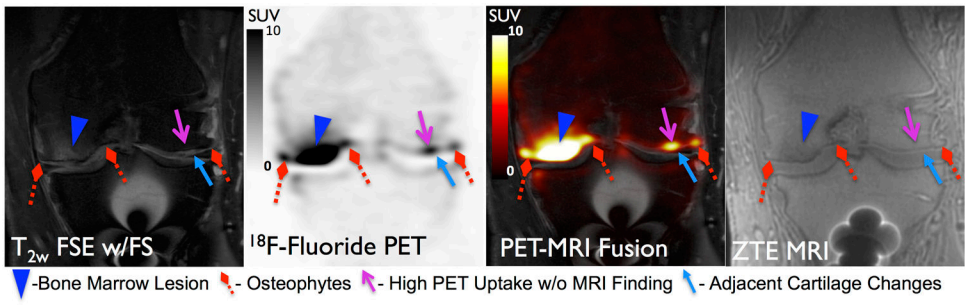


**Figure 1.**

$^{18}$F-Fluoride PET (SUV) and MRI images of a 52 year-old male patient with post-traumatic osteoarthritis showing concordance between a BML (blue arrowhead) and osteophytes (red diamond arrows) on MRI with high $^{18}$F-Fluoride uptake on PET. Additionally a focal region of high uptake on PET (magenta line arrow) did not exhibit bone abnormalities on MRI but was adjacent to a grade 2 cartilage defect (light blue solid arrow).

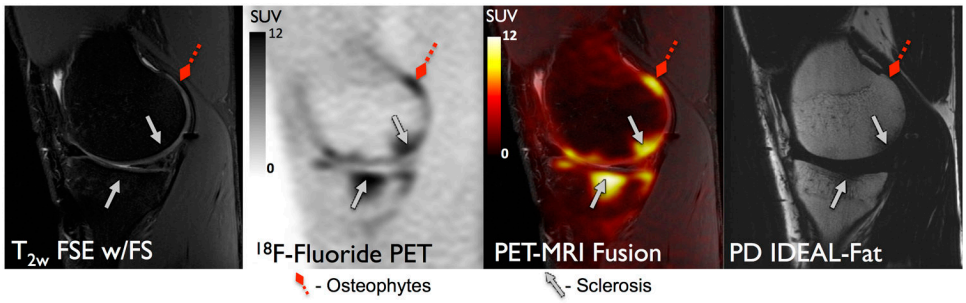


**Figure 2.**

$^{18}$F-Fluoride PET (SUV) and MRI images of a 23 year old male patient with post-traumatic osteoarthritis showing concordance between an osteophyte (red diamond arrow) and sclerosis (gray solid arrows) on MRI with high $^{18}$F-Fluoride uptake on PET.

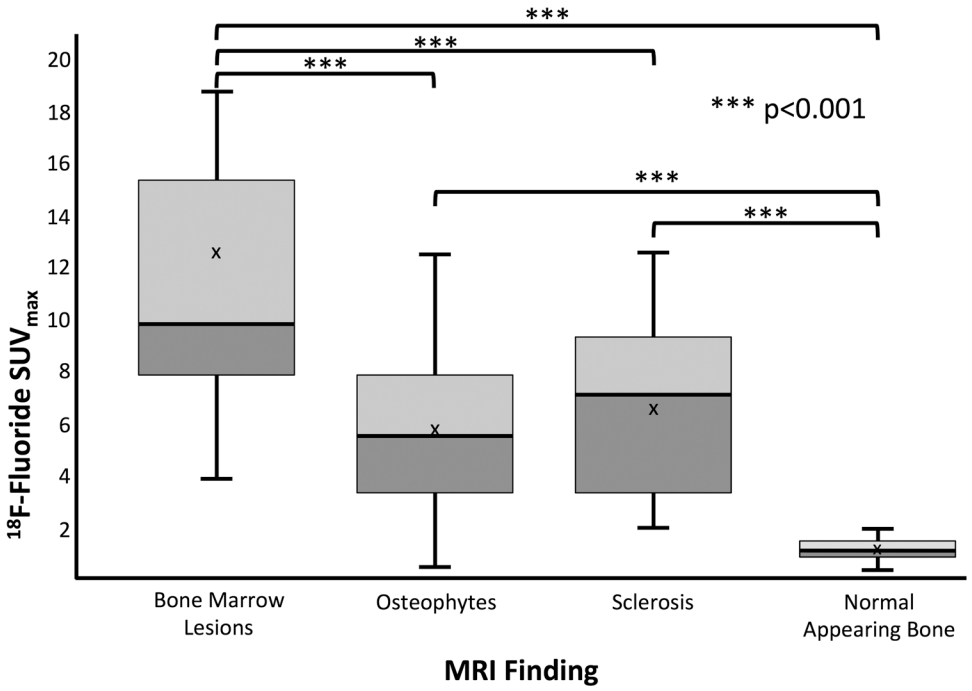


**Figure 3.**

$SUV_{max}$ distributions associated with MRI findings as a function of each type of bony abnormalities as well as normal appearing bone. BMLs showed significantly higher $^{18}$F-fluoride uptake compared to other pathology. $^{18}$F-fluoride uptake in areas of subchondral bone abnormalities identified on MRI was significantly greater than that of normal-appearing bone.

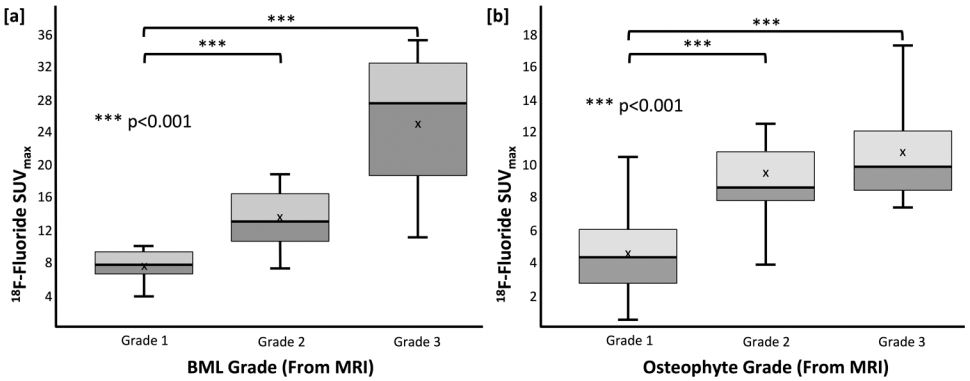


**Figure 4.**

$SUV_{max}$ distribution as a function of [a] BML grade and [b] osteophyte grade as determined on MRI findings. Significant differences were also observed between lesion grade on MRI, and PET uptake. The sensitivity of $^{18}$F-fluoride may be able to improve understanding and characterizations of these lesions

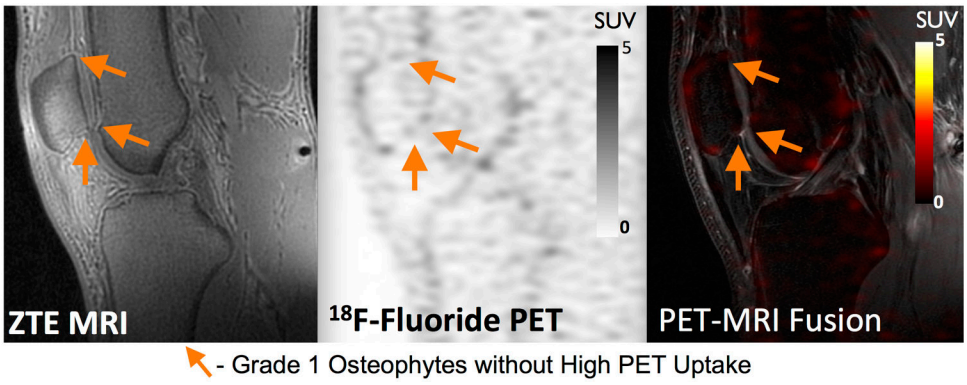


**Figure 5.**

$^{18}$F-Fluoride PET (SUV) and MRI images of a 25 year old male patient with early stage OA. Several small osteophytes identified on MR do not correlate with high $^{18}$F PET uptake (orange solid arrows).

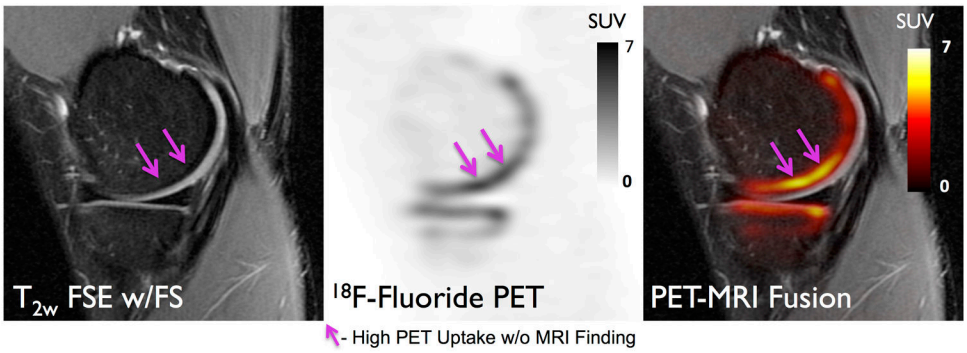


**Figure 6.**

$^{18}$F-Fluoride PET (SUV) and MRI images of a 27 year-old female patient with early stage osteoarthritis (OA). High uptake on PET (magenta line arrows) is seen in subchondral bone which does not correlate with MR findings. This may suggest that metabolic abnormalities in the bone occur prior to structural changes are seen on MRI.

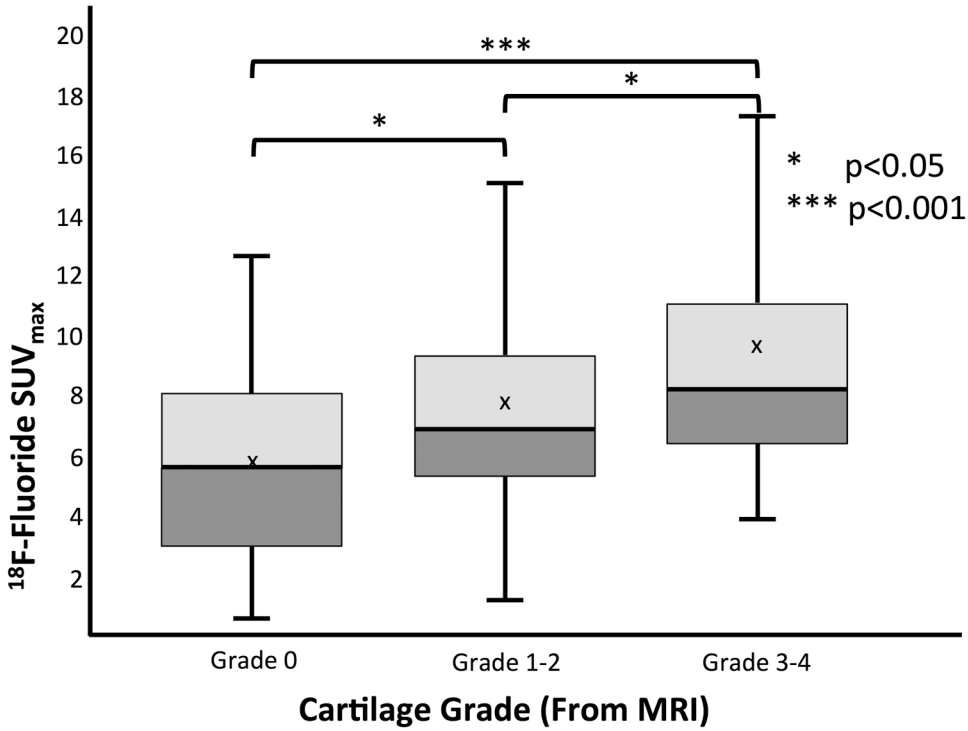


**Figure 7.**

$SUV_{max}$ distribution of $^{18}$F-Fluoride uptake as a function of adjacent cartilage grade evaluated on MR images.

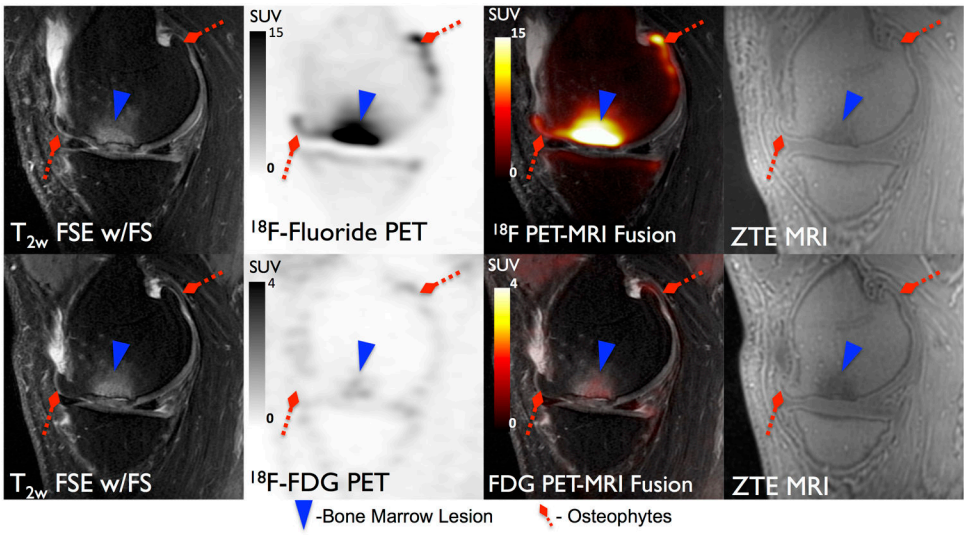


**Figure 8.**

$^{18}$F-Fluoride (Top row) and $^{18}$F-FDG (Bottom row) PET SUV maps and corresponding MR images for a 52 year-old male subject. A large grade 3 BML (Blue Arrowhead) is present on MRI which corresponds to considerably elevated uptake of $^{18}$F-Fluoride ($SUV_{max}$ =26.2) and only marginally elevated uptake of $^{18}$F-FDG ($SUV_{max}$ =1.4) relative to normal appearing bone on MRI.

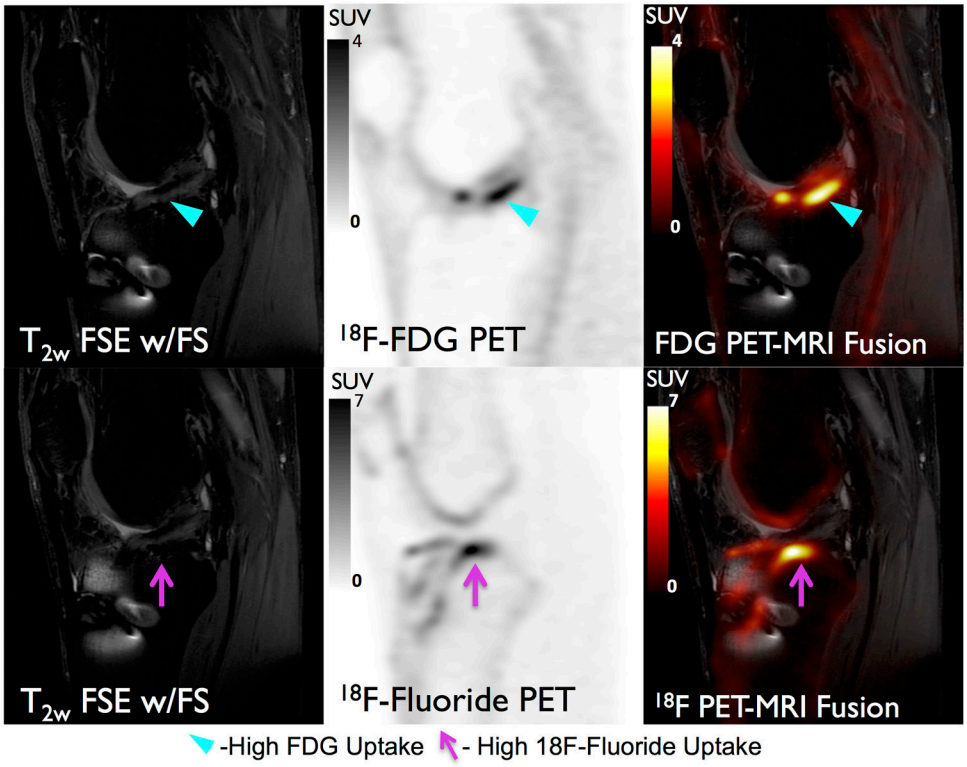


**Figure 9.**

$^{18}$F-FDG (Top) and $^{18}$F-Fluoride (Bottom) PET SUV maps and corresponding MR images for a 23 male year-old subject. Increased $^{18}$F-FDG uptake (cyan arrow) is observed around the graft that may be indicative of graft impingement or revascularization. Additionally, increased $^{18}$F-Fluoride uptake (magenta arrow) indicative of bone remodeling is seen adjacent to the graft. $^{18}$F-fluoride and $^{18}$F-FDG provide complementary information regarding subchondral bone remodeling and soft tissue inflammation and could potentially be utilized together to study OA degeneration in the entire joint.

**Table 1**

**Mean and standard deviation of $SUV_{max}$ between bone pathology as well as concordance between MRI findings and high uptake on PET ($VOI_{High}$) and mean adjacent cartilage grade**

| Finding | Mean $^{18}$F-Flouride $SUV_{max}$ | Standard Deviation | MRI Findings | MRI - $^{18}$F-Flouride Correlates | Mean Adjacent Cartilage Grade | Standard Deviation |
|---|---|---|---|---|---|---|
| **BML** | 12.4 | 6.7 | 34 | 33 | 2.3 | 1.0 |
| **Osteophyte** | 5.7 | 3.3 | 103 | 60 | 1.5 | 1.1 |
| **Sclerosis** | 6.5 | 3.2 | 13 | 8 | 1.2 | 0.8 |